

GPU-acceleration with OpenACC for an 3D Tokamak MHD code (CLT)

H. W. Zhang¹, J. Zhu¹, Z. W. Ma^{1*}, G. Y. Kan², X. Wang¹ and W. Zhang¹

¹ Institute for Fusion Theory and Simulation, Zhejiang University, Hangzhou 310027, China.

² Research Center on Flood & Drought Disaster Reduction of the Ministry of Water Resources, Beijing, China.

Abstract: The OpenACC programming model has been applied in the 3D tokamak magnetohydrodynamics (MHD) code (CLT) successfully. Great speedup has been achieved on single TITAN Xp and TITAN V GPUs with very few modifications done on the source code. And the combination of OpenACC with MPI makes the multiple GPUs parallel program feasible. The validity of the double precision operations on above two graphics cards has been checked strictly with the simulations of $m/n=2/1$ resistive tearing mode instability in tokamak. The implementation of OpenACC in CLT code, its performance test and benchmark will be introduced in detail.

Keywords: OpenACC, MPI, GPU, Magnetohydrodynamics (MHD)

* Author to whom correspondence should be addressed: zwma@zju.edu.cn

1. Introduction

Computer simulation is more and more popular in magnetic confined fusion research because the device like tokamak[1] and stellarator[2] under study are too complex to be studied analytically. And due to the restrict on computational capabilities of single processor core, parallel programming plays a major role in the acceleration of programs. Multiple parallel acceleration methods, such as MPI[3] and OpenMP[4] have been developed in the past decades. In the recent years, benefitting from the rapid performance improvement of GPU, new methods like CUDA[5], OpenCL[6] and OpenACC[7] have been developed greatly.

OpenACC as a user-driven directive-based performance-portable parallel programming model, is developed to simplify the parallel program for scientists and engineers. Compared with the CUDA and OpenCL that requires large work on rewriting code, OpenACC has many features, such as great acceleration with very few modifications on the source code, and the good compatibility with other compilers based on CPU. It has been successfully applied on some scientific and engineering codes, like the flow code NeK5000[8], the computational electromagnetics code Nekton[9], the Gyrokinetic Toroidal Code (GTC)[10], the C++ flow solver ZFS[11], and so on. And there is still great potential for the application of OpenACC in other areas.

CLT code is recently developed for the simulation of MHD instability in toroidal devices like tokamak.[12, 13] For the low parallel efficiency in accelerating the MHD code with MPI and OpenMP, OpenACC has been successfully applied in CLT code lately and we have obtained good acceleration effect on Nvidia TITAN Xp and TITAN V GPUs. Compared with the speed of a same case executed on CPU with 64 cores MPI-parallelization, about four times of acceleration has been achieved on a single TITAN V graphics card. And the correctness of result calculated on GPU is demonstrated strictly.

The detailed implementation of OpenACC and its benchmark will be introduced in this paper. And the following paper is organized as follows, In Sec. 2, the MHD model and the main modules of the CLT code will be introduced. In Sec. 3, the OpenACC implementation combined with MPI will be given. And the acceleration performance for

the CLT with OpenACC is analyzed in Sec. 4. The Sec.5 gives the benchmark for the correctness of OpenACC accelerated code. Finally, conclusion and discussion are given in Sec. 6.

2. CLT code review

CLT code with a full name of Ci-Liu-Ti (磁流体 in Chinese, and Magnetohydrodynamics in English), is an initial value full MHD code in toroidal geometries focusing on the MHD stabilities in toroidal devices like tokamak. The code is written in FORTRAN 90 with double precision format and it has grown to more than 20,000 lines with hundreds of subroutines and subfunctions. CLT code has been successfully applied in studying the influence of toroidal rotation[12], external driven current[14, 15] and Hall effect[13] on resistive tearing modes in tokamaks. And its hybrid kinetic-magnetohydrodynamic version code CLT-K has also been used in investigating nonlinear dynamics of toroidal Alfvén eigenmodes in tokamak.[16]

2.1 Basic MHD equations

The full set of resistive MHD equations including dissipations is given as follows:

$$\partial_t \rho = -\nabla \cdot (\rho \mathbf{v}) + \nabla \cdot [D \nabla (\rho - \rho_0)], \quad (1.1)$$

$$\partial_t p = -\mathbf{v} \cdot \nabla p - \Gamma p \nabla \cdot \mathbf{v} + \nabla \cdot [\kappa (p - p_0)], \quad (1.2)$$

$$\partial_t \mathbf{v} = -\mathbf{v} \cdot \nabla \mathbf{v} + (\mathbf{J} \times \mathbf{B} - \nabla p) / \rho + \nabla \cdot [\nu (\mathbf{v} - \mathbf{v}_0)], \quad (1.3)$$

$$\partial_t \mathbf{B} = -\nabla \times \mathbf{E}, \quad (1.4)$$

with

$$\mathbf{E} = -\mathbf{v} \times \mathbf{B} + \eta (\mathbf{J} - \mathbf{J}_0) + \frac{d_i}{\rho} (\mathbf{J} \times \mathbf{B} - \nabla p), \quad (1.5)$$

$$\mathbf{J} = \nabla \times \mathbf{B}, \quad (1.6)$$

where ρ , p , \mathbf{v} , \mathbf{B} , \mathbf{E} , and \mathbf{J} are the plasma density, thermal pressure, plasma velocity, magnetic field, electric field, and current density, respectively. $\Gamma (= 5/3)$ is the

ratio of specific heat of plasma. All variables are normalized as follows: $\mathbf{B} / B_m \rightarrow \mathbf{B}$,

$$\mathbf{x} / a \rightarrow \mathbf{x} , \quad \rho / \rho_m \rightarrow \rho , \quad \mathbf{v} / v_A , \quad t / \tau_a \rightarrow t , \quad p / (B_m^2 / \mu_0) \rightarrow p ,$$

$\mathbf{J} / (B_m / \mu_0 a) \rightarrow \mathbf{J}$, $\mathbf{E} / (v_A B_m) \rightarrow \mathbf{E}$, and $\eta / (\mu_0 a^2 / \tau_a) \rightarrow \eta$, where $\tau_a = a / v_A$ is the Alfvénic time, $v_A = B_m / (\mu_0 \rho_m)^{1/2}$ is the Alfvénic speed, B_m and ρ_m are the magnetic field and plasma density at the magnetic axis, and a is the half width of the plasma cross-section in the midplane.

For the equilibrium, the following equations should be satisfied:

$$\nabla \cdot (\rho_0 \mathbf{v}_0) = 0 , \quad (1.7)$$

$$\mathbf{v}_0 \cdot \nabla p_0 + \Gamma p_0 \nabla \cdot \mathbf{v}_0 = 0 , \quad (1.8)$$

$$\rho_0 \mathbf{v}_0 \cdot \nabla \mathbf{v}_0 = \mathbf{J}_0 \times \mathbf{B}_0 - \nabla p_0 , \quad (1.9)$$

$$\nabla \times \mathbf{E}_0 = 0 . \quad (1.10)$$

Substituting these equilibrium equations into Equations(1.1)-(1.4), the MHD equations can be rewritten as

$$\partial_t \rho = -\nabla \cdot (\rho \mathbf{v}_1 + \rho_1 \mathbf{v}_0) + \nabla \cdot [D \nabla (\rho - \rho_0)] , \quad (1.11)$$

$$\partial_t p = -\mathbf{v}_1 \cdot \nabla p - \mathbf{v}_0 \cdot \nabla p_1 - \Gamma (p \nabla \cdot \mathbf{v}_1 + p_1 \nabla \cdot \mathbf{v}_0) + \nabla \cdot [\kappa (p - p_0)] , \quad (1.12)$$

$$\begin{aligned} \partial_t \mathbf{v} = & -(\mathbf{v} \cdot \nabla \mathbf{v}_1 + \mathbf{v}_1 \cdot \nabla \mathbf{v}_0 + \rho_1 \mathbf{v}_0 \cdot \nabla \mathbf{v}_0 / \rho) \\ & + (\mathbf{J}_1 \times \mathbf{B} + \mathbf{J}_0 \times \mathbf{B}_1 - \nabla p_1) / \rho + \nabla \cdot [\nu (v - v_0)] , \end{aligned} \quad (1.13)$$

$$\partial_t \mathbf{B} = -\nabla \times \mathbf{E}_1 , \quad (1.14)$$

where the variables with subscript 0 represent equilibrium components and 1 for perturbation components, e.g., $\mathbf{v}_1 = \mathbf{v} - \mathbf{v}_0$. Thus, numerical errors from equilibrium can be minimized.

2.2 Coordinate systems and numerical schemes

In CLT, the cylindrical coordinate system (R, ϕ, Z) , is chosen, as shown in Figure 1.

Besides the outer magnetic surface, a $m/n=3/1$ magnetic island inside calculated by CLT code is also plotted in three dimensions. In the toroidal geometry device like tokamak, R , ϕ and Z indicate the major radius, toroidal, and up-down directions, respectively. One advantage this coordinate system is that one can avoid the singularity near $r = 0$ point that occurs in the toroidal coordinate (ψ, θ, ζ) . However, the outer boundary handling would be more difficult in cylindrical coordinate. In the last version of CLT, the plasma boundary at the last flux surface of plasma is assumed to be fixed. And recently, the cut-cell method has been applied in CLT successfully, the details for the new boundary handling method will be introduced in another paper.

The grids are dispersed in R , ϕ and Z direction and are rectangular in $R-Z$ plane. The 4th order finite difference method is employed in R and Z directions, while in ϕ direction, either finite difference or pseudo-spectrum method can be used. As for the time-advance, 4th order Runge-Kutta scheme is chosen.

For the parallelization on CPU platform, the simulation domain can be divided into multiple blocks in each direction, and four-layer grids will be used for message passing between every two neighboring blocks due to the chosen of 4th order finite difference method spatially. Thus, the increasement on MPI cores with a fixed problem size will leads to the rapid decay of parallel efficiency.

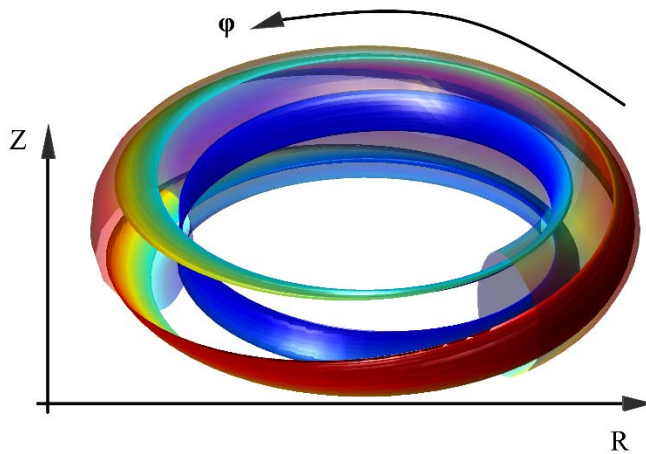


Fig. 1. Sketch of cylindrical coordinate system (R, ϕ, Z) in a toroidal geometry device. A $m/n=3/1$ magnetic island inside the outer magnetic surface calculated by CLT code is plotted

in three dimensions.

2.3 Main modules and the basic flow of CLT

For each iterative step of CLT, 8 components of $\rho, p, \mathbf{v}, \mathbf{B}$ need to be updated. The main processes of CLT is shown in Figure 2. The modules with red squares are executed on CPU, while the blue ones on GPU, and the green squares mark out the main OpenACC directives in the whole procedure. The **INITIAL** module reads the equilibrium files that are calculated by equilibrium code, like NOVA[17] and EFIT.[18] Then the **DERIVATIVES OF $\rho, p, \mathbf{v}, \mathbf{B}$** module is called with the spatial differential scheme mentioned above. With these derivatives, the value of current and electric field \mathbf{J}, \mathbf{E} is obtained. Then the derivatives, \mathbf{J} and \mathbf{E} are substituted into the **RIGHT HANDS OF EQUATIONS**, and finally $\rho, p, \mathbf{v}, \mathbf{B}$ are updated in **STEP ON** module with the 4th order Runge-Kutta scheme. Note that, during the iteration, the **BDOUNDARY** module is applied in each step to solve the boundary conditions and deal with data exchange due to MPI parallelization, while the **TIME STEP** module calculate the time step length based on the latest $\rho, p, \mathbf{v}, \mathbf{B}$ to satisfy the CFL condition on all grids, and some other modules like **DIAGN** (data analysis) and **OUTPUT** (data record) are called every few steps.

The executing time of CLT code is mostly spent on the **RIGHT HANDS OF EQUATIONS**, **DERIVATIVES OF $\rho, p, \mathbf{v}, \mathbf{B}$** and \mathbf{J}, \mathbf{E} modules. Therefore, a large majority of OpenACC directives are added in these modules.

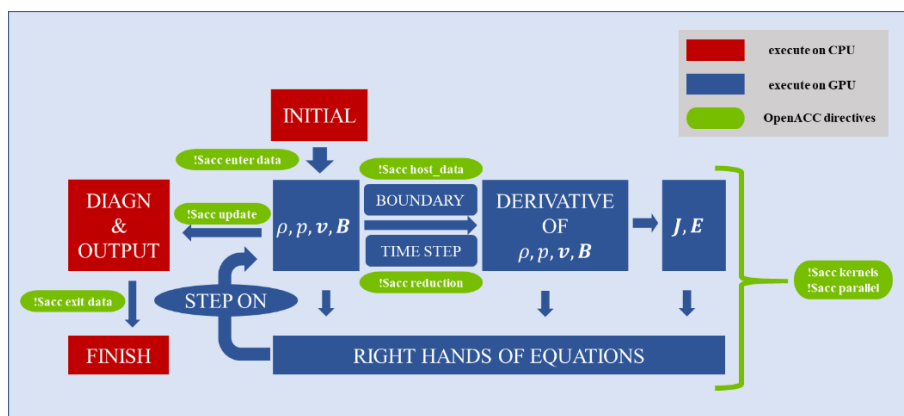


Fig. 2. Main modules and OpenACC directives of CLT code. The modules in blue blocks are executed on GPU, and those in red blocks are on CPU. The green blocks indicate the

OpenACC directives applied in the corresponding position.

3. OpenACC and MPI implementation in CLT code

3.1 OpenACC directives in the serial version CLT code

The main idea of GPU-acceleration using OpenACC is to transfer the calculation process from CPU to GPU. And the data interaction speed between the memories of CPU and GPU is much slower than the self-memory access. Thus, the first important operation is to copy all variables required in iteration to the graphic memory. After the **INITIAL** module reads the equilibrium files, all necessary variables are copied into the graphic memory by using '*\$acc enter data copyin(variable names)*' directive as shown in Figure 2. Accordingly, after finishing all iterations, the '*\$acc exit data delete(variable names)*' directive is also used before the program finishing to free the graphic memory. There are also other methods play the same role, such as combination of '*!\$acc declare create(variable names)*' and '*!\$acc update device(variable names)*'. The main advantage of '*enter data*' and '*declare create*' construct is that the data lifetime in the graphic memory can be extended crossing subfunctions and subroutines. With this feature, the calculation on GPU can be continuously proceeded without stopping for data transferring with CPU.

An example for the '*enter data*' constructs in CLT is given in Figure 3. For simplicity, only three variables (*xx, yy, zz*) are listed in the OpenACC directives. During the main iterations, CLT program will have to call the **DIAGN** and **OUTPUT** modules every few steps to analyze data and record it into disk files by CPU. Because **DIAGN** is quite complex and depends on some external math library, such as MKL[19], this module is still executed on CPU for the difficulty in parallelization with OpenACC. Therefore, just before calling the **DIAGN** and **OUTPUT** module, the directive '*!\$acc update host(variable names)*' is used to copy the latest data from GPU to CPU. The time waste on updating operation is negligible because the number of calls on these two modules is much smaller than the total iteration steps.

```

1  program CLT
2      ! initialize
3      call initia
4
5      !$acc enter data copyin(xx,yy,zz)
6
7      ! main iteration part
8      do nstep=1,nstop
9          call stepon
10         if(mod(nstep,ndiagn)==0) then
11             !$acc update host(xx,yy,zz)
12             call diagn
13         endif
14         if(mod(nstep,noutput)==0) then
15             !$acc update host(xx,yy,zz)
16             call output
17         endif
18     enddo
19     !$acc exit data delete(xx,yy,zz)
20
21 end program CLT

```

Fig. 3. A simple example for ‘enter data’ and ‘update’ constructs in CLT.

```

1  subroutine setdt
2      use declare
3      include 'mpif.h'
4      dt1=100.
5      !$acc parallel present(x,xx,yy,zz,gdtp_ep)
6      !$acc loop reduction(min:dt1) independent collapse(3)
7      do jy=iy_first+2, iy_last-2
8      do jz=iz_first+2, iz_last-2
9      do jx=ix_first+2, ix_last-2
10         if(gdtp_ep(jx,jz,1).ne.4) then
11             vx=x(jx,jz,jy,3)*x(jx,jz,jy,6)**2/x(jx,jz,jy,1)
12             vy=x(jx,jz,jy,4)*x(jx,jz,jy,7)**2/x(jx,jz,jy,1)
13             vz=x(jx,jz,jy,5)*x(jx,jz,jy,8)**2/x(jx,jz,jy,1)
14             va2=(x(jx,jz,jy,6)**2*x(jx,jz,jy,7)**2 +
15                  +x(jx,jz,jy,8)**2)/x(jx,jz,jy,1)
16             cs2=gamma*x(jx,jz,jy,2)/x(jx,jz,jy,1)
17             vpx=dabs(vx)+sqrt(dabs(cs2+va2))
18             vpy=dabs(vy)+sqrt(dabs(cs2+va2))
19             vpz=dabs(vz)+sqrt(dabs(cs2+va2))
20             dtx=dabs(xx(jx)-xx(jx-1))/(vpx/cfl)
21             dtz=dabs(zz(jz)-zz(jz-1))/(vpz/cfl)
22             dty=dabs(xx(jx)*(yy(jy)-yy(jy-1)))/(vpy/cfl)
23
24             dt2=dmin1(dtx,dtz)
25             dt3=dmin1(dty,dt2)
26             dt1=dmin1(dt1,dt3)
27         endif
28     enddo
29   enddo
30 enddo
31 !$acc end parallel
32 return
33 end subroutine setdt

```

Fig. 4. A section for the parallelization of the module Time Step using ‘parallel’ constructs.

Inside the **STEP ON** module, simple transversal differential calculations on each grid for the right hand of equations occupy the major part. In most cases, three levels of loops are used in the code for the three-dimensional situation. To parallelize the loops, two constructs of ‘kernels’ and ‘parallel’ are frequently used. A section for the parallelization of the TIME STEP module is given in Figure 4 as a representative example. The ‘present’ clause following ‘parallel’ construct directive indicates compiler that the variables inside

the parentheses already exist in the GPU, so as to avoid the needless implicit variable copy or create operations in the GPU. And the ‘*loop*’ clause after ‘*parallel*’ directive should be placed just before the loop body, this clause tells the compiler the closely followed loop can be parallelized. As for the **TIME STEP** module, the final time step length should satisfy the CFL condition in each grid, therefore, the reduction for the minimum time step length is used by adding ‘*reduction(min:dt1)*’. Other reduction operations are also supported in OpenACC with similar syntaxes.[7] The ‘*independent*’ clause tells the compiler that the calculation on each grid has no dependency and therefore can be parallelized directly. The final one clause in Figure 4 is ‘*collapse(3)*’. Collapsing loops means that, for example, three loops of trip counts NX, NZ and NY respectively will be automatically turned into a single loop with a trip total count of NX*NZ*NY, which is usually beneficial to the parallelization. Note that the ‘*parallel*’ constructs used here can also be replaced by ‘*kernel*s’ construct, the major difference of these two constructs is that ‘*kernel*s’ gives the compiler more freedom to find and map parallelism according to the requirements of the target accelerator, while the parallel construct is more explicit, and requires more analysis by the programmer.

Another important OpenACC directive used in CLT is the ‘*!\$acc routine*’ directive for the procedure call. Figure 5 gives the solution when a subroutine or function is called inside an accelerated loop. The subroutine ‘*interp1d2l*’ calculates a simple interpolation with a given data series, and is commonly used in the accelerated region of **BOUNDARY** module. The ‘*!\$acc routine seq*’ directive requires the compiler to generate a copy version for this subroutine on GPU so that it can be called in the accelerated region. And an interface for this child subroutine is required inside the parent as given in Figure 5. Then the subroutine can be called inside the OpenACC accelerated region directly.

```

1  subroutine interp1d2l(x1,x2,x3,y1,y2,y3,y,ans)
2      !$acc routine seq
3      real*8 x1,x2,x3,y1,y2,y3,y,ans
4      real*8 d1,d2,d3
5      d1 = (y1-y2)*(y1-y3)
6      d2 = (y2-y3)*(y2-y1)
7      d3 = (y3-y1)*(y3-y2)
8      ans = x1*(y-y2)*(y-y3)/d1 &
9          + x2*(y-y3)*(y-y1)/d2 &
10         + x3*(y-y1)*(y-y2)/d3
11      return
12  end subroutine interp1d2l
13
14  subroutine boundary
15      use declare
16      implicit none
17      include 'mpif.h'
18
19      ! interface for accelerated subroutine
20      interface
21          subroutine interp1d2l(x1,x2,x3,y1,y2,y3,y,ans)
22          !$acc routine seq
23          real*8 x1,x2,x3,y1,y2,y3,y,ans
24          real*8 d1,d2,d3
25          end subroutine interp1d2l
26      end interface
27
28      ! OpenACC accelerated region
29      .....
30      call interp1d2l(x1,x2,x3,y1,y2,y3,y,ans)
31      .....
32  end subroutine boundary

```

Fig. 5. An example for the procedure (subroutine interp1d2l) call inside OpenACC accelerated region.

3.2 Combination of OpenACC and MPI for multiple GPU parallelization

The CLT code was developed with MPI API at first for parallelization in clusters. For ordinary cases we used as (256, 256, 16) grids in (R, Z, ϕ) directions, the graphic memory usage in graphics card is about 1.45GB, thus, the memory in a single graphics card like TITAN Xp or TITAN V (with 12GB graphic memory) is more than enough for a typical CLT case. However, considering the future extensibility for studying larger size problems like the high n modes in tokamak, a size of (1024, 1024, 128) grids or even larger will be necessary. In such situations, more than 128 times memory (over 166GB) will be required in GPU and the multiple GPU parallelization will be indispensable. Based on the original MPI API in CLT, we also added the directives for the directly commutation between devices without transferring data back to the host.

As shown in Figure 6, firstly, we add the ‘`!$acc set device_num(rank of GPU)`’ directive just after the ‘`mpi_comm_size`’ and ‘`mpi_comm_rank`’ calls. The value of ‘`rank of GPU`’ can be defined as functions of the process rank in MPI parallelization so that each MPI rank can be assign to different GPUs for the load balance. With this ‘`rank of`

GPU', the commutation between different GPU becomes possible. Then, a specific example with OpenACC directives in ‘*mpi_send*’ and ‘*mpi_recv*’ API is given. The ‘*!\$acc host_data use_device(variable names) if_present*’ tells the compiler to use the address of the specified variables on GPU if the variables are present, then the ‘*mpi_send*’ or ‘*mpi_recv*’ API is executed by accessing the data from the GPU address of variable rather the CPU. The using of ‘*host_data use_device*’ avoids the unnecessary data transfer between CPU and GPU before MPI calls. For comparison, an equivalent example is given is Figure 7, where the MPI API still accesses the data from the CPU address for specified variables. However, to update the data inside the CPU and GPU, another pair of ‘*!\$acc update host(variable names)*’ and ‘*!\$acc update device(variable names)*’ are added before the ‘*mpi_send*’ and after the ‘*mpi_recv*’, respectively. The functions of the methods used in Figure 6 and Figure 7 are the same, but the later one will spend additional time on updating data between CPU and GPU.

```

1  program CLT
2  .....
3  ! initiate mpi
4  call mpi_init(ierr)
5  call mpi_comm_size(MPI_COMM_WORLD, nsize, ierr)
6  call mpi_comm_rank(MPI_COMM_WORLD, nrank, ierr)
7  !$acc set device_num(0)
8
9 .....
10 !mpi -----
11 !$acc host_data use_device(wfx1) if_present
12 call mpi_send( wfx1, myz8, MPI_DOUBLE_PRECISION, nrank + 1, 0,  &
13 | | | MPI_COMM_WORLD, ierr )
14 !$acc end host_data
15 .....
16 !mpi -----
17 !$acc host_data use_device(wfx1,wfx2) if_present
18 call mpi_recv( wfx1, myz8, MPI_DOUBLE_PRECISION, nrank - 1, 0,  &
19 | | | MPI_COMM_WORLD, status, ierr )
20 !$acc end host_data
21 .....
22 end program CLT
23

```

Fig. 6. An example for MPI API called on GPU by using ‘*host_data use_device*’ construct.

```

1  program CLT
2  .....
3  ! initiate mpi
4  call mpi_init(ierror)
5  call mpi_comm_size(MPI_COMM_WORLD,nsize,ierror)
6  call mpi_comm_rank(MPI_COMM_WORLD,nrank,ierror)
7  !$acc set device_num(0)
8
9  .....
10 !mpi  -----
11 !$acc update host(wfx1)
12 call mpi_send( wfx1, myz8, MPI_DOUBLE_PRECISION, nrank + 1, 0,  &
13 | | | | | MPI_COMM_WORLD,ierror )
14 .....
15 !mpi  -----
16 !$acc update device(wfx1)
17 call mpi_recv( wfx1, myz8, MPI_DOUBLE_PRECISION, nrank - 1, 0,  &
18 | | | | | MPI_COMM_WORLD, status,ierror )
19 .....
20 end program CLT

```

Fig. 7. An example for MPI API called on CPU by using ‘update’ construct..

4. Acceleration performance analysis

For the most common case with grids set as (256, 256, 16) in R , Z and ϕ we used in simulation, the comparison for execution time (with 20,000 steps) is given for different platforms in Figure 8. The MPI block division for CPU version code is carried out uniformly in R and Z directions, while no block division is applied in the GPU version because we only used one card for acceleration. Note that for the cases executing on the CPU, the ‘O3’ compiler option is turned on so as to obtain the best speed performance. And the test for CPU case is carried out on the cluster KYLIN-2 in our institute, with total 138 nodes and 2 Intel® Xeon® Gold 6148F CPUs for each node (40 cores in each node), while the case for GPU test is performed on several workstations with single NVIDIA GPU installed on each.

As we can see in Figure 8, the performance of the code based on MPI executed on CPU is still acceptable when total 128 cores (4 nodes) are used, with the parallel efficiency about 70%. However, the efficiency drops quickly to 45% when the number of CPU cores is increased to 256 (7 nodes). The reason for the decline of parallel efficiency with the increasing of CPU cores is mainly due to the growth of the overlap area between different MPI blocks for the usage of fourth order central difference scheme spatially. Therefore, the speedup for MHD code with a fixed problem size is quite difficult on traditional MPI frame. Fortunately, the application of OpenACC based on GPU on our CLT code results in a quite good acceleration performance.

As the results shown in Figure 8 with the green and blue bars for TITAN Xp and TITAN V, respectively, the elapsed time on TITAN Xp almost equals to that of 256 Intel® Xeon® Gold 6148F CPU cores. What's more, the speed of TITAN V is even 43% faster than that of TITAN Xp. Compared with our frequently-used MPI set of 64 cores, the speedup of TITAN V is about 3.7-fold. In addition to the speed performance, another advantage for the GPU-acceleration is the much lower price for construct GPU workstations or servers than building a cluster with nodes of CPU. The cost of a single TITAN V is comparable with one Intel® Xeon® Gold 6148F CPU (20 cores in each), thus, the cost performance of the former is about ten times better than the latter for our CLT code.

A problem for the acceleration speed for CPU-MPI and GPU-OpenACC has to be discussed here is that, the computational capability for double precision floating points of TIAN Xp is up to 0.380 TFLOPS, which is only comparable with one Intel® Xeon® Gold 6148F CPU with 20 cores (without exact data yet). But the speed on TITAN Xp is about 4 times of that on CPU with 32 cores. Besides, the computational capability of the TITAN V is about 6.9 TFLOPS, which is more than 10 times of the TITAN Xp, but the speed on TITAN V have been only accelerated less than twice compared with that on TITAN Xp. Therefore, the parallelization performance of the code on different platforms is not entirely depends on the computational capability. Other factors like the memory accessing time, bandwidth, I/O situation, compiler optimization options, and the network conditions will all affect the code's speed. And the deeper reasons for the difference of OpenACC and MPI acceleration are still under study.

The other one important feature used in OpenACC is the combination of three levels parallelization as ‘gang’, ‘work’, ‘vector’. For the test cases shown in Figure 8, we found that the speed of CLT code on the specified problem size is most sensitive to the number of ‘gang’: enough gangs parallelization (more than 512) leads to the best performance on GPU, while too few gangs (less than 100) results in even the slow down of the code compared with MPI case with 32 cores. And the default set of the compiler without adding any artificially specified number of three levels parallelization also leads to the best performance of the acceleration as shown in Figure 8. The numbers of ‘gang’, ‘worker’, ‘vector’ will affect the usage of graphic

memory cache and can influence the speed greatly. For codes accelerated with OpenACC, adjusting these numbers are necessary to obtaining the best acceleration performance, and the best set is also quite different for different code and different problem size.

And for the lack of cluster with multiple GPU nodes, the speed test for the OpenACC combined with MPI between different GPUs has not been performed yet. However, a simple test for MPI-GPU acceleration is carried out on a single TITAN Xp with 4 MPI ranks for the two implementation methods mentioned in Figure 6 and 7. The first method (as in Figure 6, with direct communication between GPU) leads to only 15% slow down compared with time showed by the green bar in Figure 8, while the other method (as in Figure 7, use ‘*update*’ clause and communication between CPU) leads to 105% slow down. Therefore, the direct communication MPI support in GPU makes the multiple GPUs acceleration for large size problems become feasible.

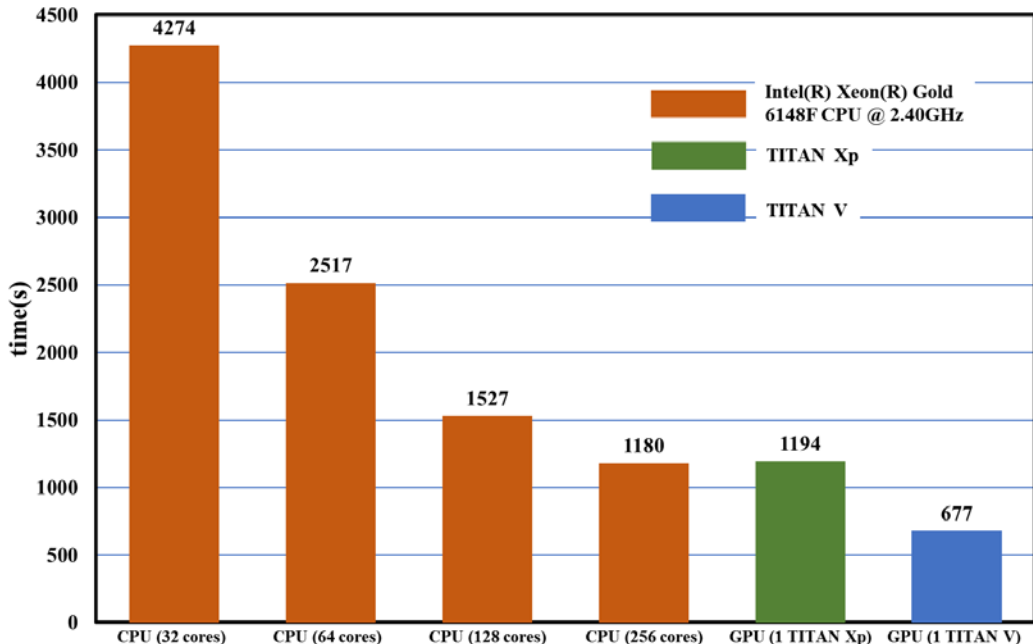


Fig. 8. Comparison for execution time on different platforms (CPU colored by orange, TITAN Xp colored by green, and TITAN V colored by blue).

5. Results benchmark

To demonstrate the validity of the results calculated by the OpenACC acceleration on GPU, the m/n=2/1 resistive tearing mode for tokamak is carried out both on the CPU-MPI platform (Intel® Xeon® Gold 6148F CPU @ 2.40GHz, 32 cores) and the GPU-OpenACC platform

(TITAN V, TITAN Xp, 1 GPU).

The initial equilibrium is calculated by the NOVA code [17] with the initial safety factor q and pressure p profile as shown in Figure 9. The $m/n=2/1$ mode is most unstable for this equilibrium. The grids set is the same as above mentioned. The resistivity η is chosen to be 1×10^{-5} .

Temporal evolution for the kinetic energy of the system is given in Figure 10 for the CPU-MPI result and GPU-OpenACC result respectively. The energy values of the two cases are exactly the same during the whole 400,000 simulation steps, except for some negligible differences on the 14th decimal place of the number, which is almost the machine error limitation of the double precision.

Besides, the mode structures calculated with two cases are identically the same, as the result of CPU-MPI case shown in Figure 11(a), and the contour plot for the difference of the mode structures by CPU and GPU is also given in Figure 11(b). The mode structure of E_ϕ in Figure 11(a) is clearly a $m/n=2/1$ mode, the result calculated by GPU-OpenACC is omitted due to the indistinguishability. The difference of the results between CPU-MPI and GPU-OpenACC as shown in Figure 11(b) is less than 10^{-14} , which is consistent with the situation of kinetic energy. As for the result in TITAN Xp, it is just the same as that in TITAN V, thus it will not be repeated here.

Therefore, the consistency for the $m/n=2/1$ tearing mode on both platforms demonstrate the reliability of GPU-OpenACC for the double precision simulation of CLT code. And the stability is also verified with dozens of simulations with each over 400,000 steps. The lack of ECC memory in TITAN Xp and TITAN V doesn't influence the correctness of the CLT results so far.

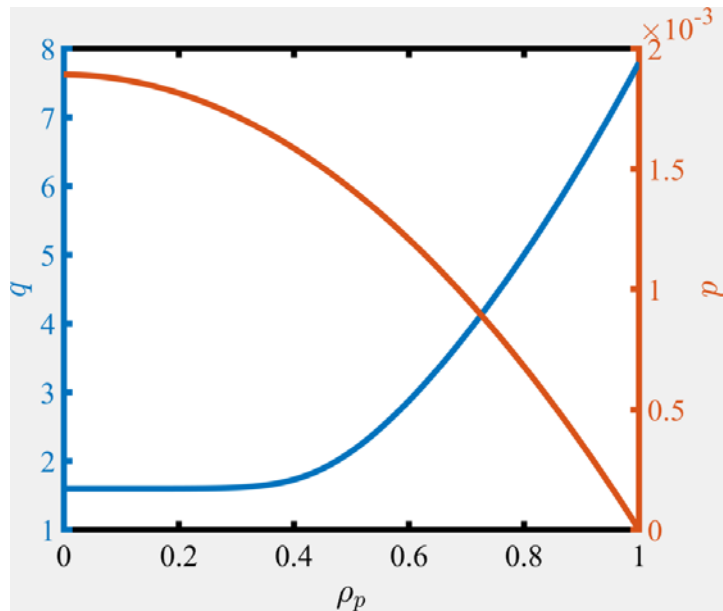


Fig. 9. Initial equilibrium safety factor q profile and pressure p profile for $m/n=2/1$ resistive tearing mode simulation.

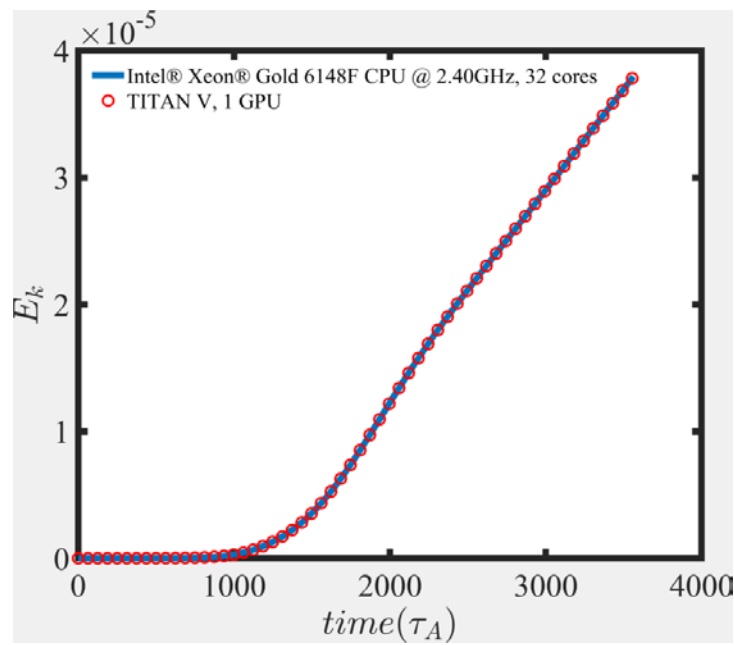


Fig. 10. Temporal evolutions for the kinetic energy of the system for two cases respectively executed on CPU-MPI platform (blue line), and GPU-OpenACC platform (red circles).

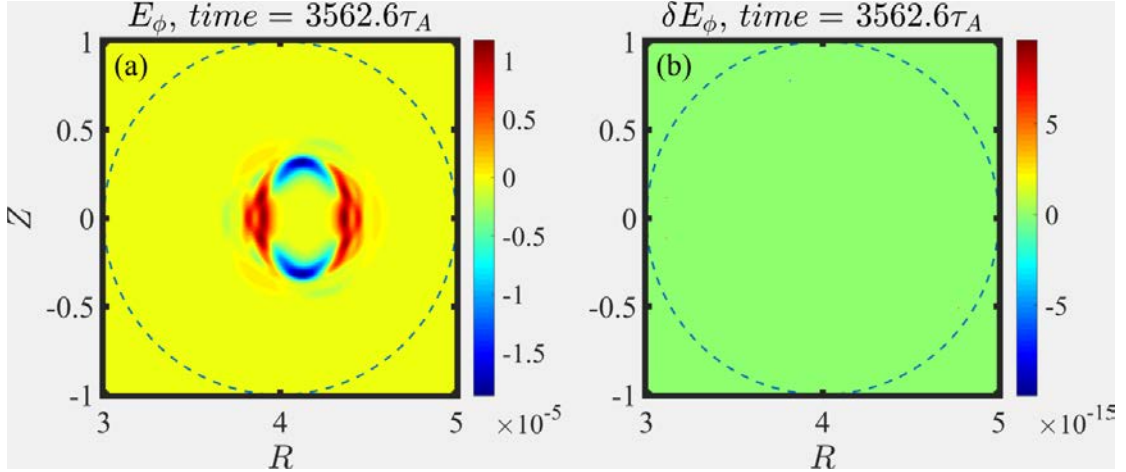


Fig. 11. (a) m/n=2/1 mode structure exhibited by E_ϕ . (b) the difference of E_ϕ between the results calculated by CPU-MPI platform and GPU-OpenACC platform.

6. Discussion and Conclusion

The success application of OpenACC in CLT code leads to great improvement in work efficiency for studying the MHD instability in tokamak. The transference for CLT code from the CPU-MPI platform to GPU-OpenACC platform is relatively easy compared with rewritten the code into CUDA or OpenCL. Only about 500 lines OpenACC directives have been added into the code, which is quite a few compared with total more than 20,000 lines. And some minor changes have been done on the code, such as merging some small subroutines and adjusting the order of cyclic indices to obtain the best acceleration performance.

Compared with the speed of a same case executed on CPU with 64 cores MPI-parallelization, about four times of acceleration has been achieved on a single TITAN V graphics card. And the combination of MPI and OpenACC makes the multiple GPUs acceleration become feasible with simply call MPI APIs with the data address on GPU memory.

The speedup is found to depending more factors than the computational capabilities of the CPU and GPU. Only about double speed of TITAN Xp is obtained on TITAN V, while the latter one's computational capability in double precision is ten times more than that of the former. Therefore, greater potential in TITAN V is seen if more optimization on the CLT code like improvement of data locality, is done. However, the speed of the code and the time spent on optimization is a trade-off. Because the speedup performance on TITAN V is already pretty

good considering its low price, and to keep the integrity and readability of code structure, acceleration work on CLT code is paused at this stage.

Most important of all, the benchmark for the results calculated by GPU are done by comparing that of traditional CPU platforms. The result is exactly correct after 400,000 steps for dozens of runs. The double-precision operations on TAN Xp and TITAN V are quite trusty for our CLT code.

By the way, the migration to OpenACC for kinetic part of hybrid kinetic-magnetohydrodynamic version code CLT-K is still under way, which requires more modification on the code structure and adjustment on the combination of different OpenACC directives. And the experience for this work on CLT-K will be introduced in a future paper if the acceleration performance is noteworthy.

Acknowledgments

The authors would like to acknowledge helpful suggestions given by professor C. Yang, and the Sunway TaihuLight Supercomputer Team at National Supercomputing Center, Wuxi.

.....

References

1. Wan, B., *Recent experiments in the EAST and HT-7 superconducting tokamaks*. Nuclear Fusion, 2009. **49**(10): p. 104011.
2. Renner, H., et al., *The capabilities of steady state operation at the stellarator W7-X with emphasis on divertor design*. Nuclear Fusion, 2000. **40**(6): p. 1083.
3. Walker, D.W. and J.J. Dongarra, *MPI: A standard message passing interface*. Supercomputer, 1996. **12**: p. 56-68.
4. Dagum, L. and R. Menon, *OpenMP: an industry standard API for shared-memory programming*. IEEE computational science and engineering, 1998. **5**(1): p. 46-55.
5. Cook, S., *CUDA programming: a developer's guide to parallel computing with GPUs*. 2012: Newnes.
6. Kaeli, D.R., et al., *Heterogeneous computing with OpenCL 2.0*. 2015: Morgan

Kaufmann.

7. Farber, R., *Parallel programming with OpenACC*. 2016: Newnes.
8. Markidis, S., et al., *OpenACC acceleration of the Nek5000 spectral element code*. The International Journal of High Performance Computing Applications, 2015. **29**(3): p. 311-319.
9. Otten, M., et al., *An MPI/OpenACC implementation of a high-order electromagnetics solver with GPUDirect communication*. The International Journal of High Performance Computing Applications, 2016. **30**(3): p. 320-334.
10. Wang, Y., et al., *Porting and optimizing gtc-p on taihulight supercomputer with sunway openacc*. HPC China, 2016.
11. Kraus, J., et al., *Accelerating a C++ CFD code with OpenACC*, in *Proceedings of the First Workshop on Accelerator Programming using Directives*. 2014, IEEE Press: New Orleans, Louisiana. p. 47-54.
12. Wang, S. and Z. Ma, *Influence of toroidal rotation on resistive tearing modes in tokamaks*. Physics of Plasmas, 2015. **22**(12): p. 122504.
13. Zhang, W., Z. Ma, and S. Wang, *Hall effect on tearing mode instabilities in tokamak*. Physics of Plasmas, 2017. **24**(10): p. 102510.
14. Wang, S., Z. Ma, and W. Zhang, *Influence of driven current on resistive tearing mode in Tokamaks*. Physics of Plasmas, 2016. **23**(5): p. 052503.
15. Zhang, W., S. Wang, and Z. Ma, *Influence of helical external driven current on nonlinear resistive tearing mode evolution and saturation in tokamaks*. Physics of Plasmas, 2017. **24**(6): p. 062510.
16. Zhu, J., et al., *Nonlinear dynamics of toroidal Alfvén eigenmodes in the presence of tearing modes*. Nuclear Fusion, 2018.
17. Cheng, C. and M. Chance, *NOVA: A nonvariational code for solving the MHD stability of axisymmetric toroidal plasmas*. Journal of Computational Physics, 1987. **71**(1): p. 124-146.
18. Lao, L., et al., *Reconstruction of current profile parameters and plasma shapes in tokamaks*. Nuclear fusion, 1985. **25**(11): p. 1611.

19. Wang, E., et al., *Intel math kernel library*, in *High-Performance Computing on the Intel® Xeon Phi™*. 2014, Springer. p. 167-188.